

# Analysis of Factors Influencing the Corrosion Rate of Reinforcing Steel Bars in Concrete: A Ranking Study

Mohamed Fergany Badawy<sup>1,\*</sup>, Mohamed Saif<sup>2</sup>, Mohamad Osama Ramadan Al Hariri<sup>2</sup>,  
Hossameldin hamad<sup>2</sup>, Ahmed Serag<sup>3</sup>, Ghada Abd El-Hafez<sup>4</sup>

<sup>1</sup> Department of Civil Engineering, Higher Institute of Engineering, 15th May City, Cairo, Egypt.

<sup>2</sup> Department of Civil Engineering, Faculty of Engineering at Shoubra, Benha University, Cairo, Egypt.

<sup>3</sup> Department of Civil Engineering, Faculty of Engineering, Fayoum University.

<sup>4</sup> Department of Chemistry, Faculty of Science, Fayoum University.

\*Corresponding author

E-mail address: fergany2017@yahoo.com, mohamed.ismaeel@feng.bu.edu.eg, osama.alhariri@feng.bu.edu.eg,  
hossameldin.hamad@feng.bu.edu.eg, asg00@fayoum.edu.eg, gma03@fayoum.edu.eg

**Abstract:** Corrosion of steel reinforcement in concrete is a significant concern that affects the durability and service life of reinforced concrete structures. This study investigates the factors influencing the corrosion rate of steel bars embedded in concrete, focusing on key material properties such as penetration depth, alkalinity, compressive strength, tensile strength, and sorptivity. Fourteen concrete mixes, including supplementary cementitious materials (SCMs) such as silica fume, fly ash, and slag, were tested under accelerated corrosion conditions using a 3.5% sodium chloride solution. Statistical analysis was performed using SPSS software to evaluate the relationships between these variables and the corrosion rate. The results revealed that penetration depth had the strongest positive correlation with corrosion, while alkalinity and compressive strength exhibited significant negative correlations, highlighting their protective roles. Tensile strength and sorptivity showed moderate correlations with corrosion rate. Among the tested mixes, those incorporating SCMs, particularly silica fume, demonstrated superior corrosion resistance due to improved microstructure and reduced permeability. This study emphasizes the importance of optimizing concrete mix designs and utilizing SCMs to enhance the durability of concrete structures exposed to aggressive environments.

**Keywords:** Corrosion Rate, Corrosion Resistance, Cementitious Materials, Penetration Depth, Alkalinity.

## 1. Introduction

Corrosion of reinforcement steel within reinforced concrete structures is a critical issue that significantly impacts durability and reduces the service life of these structures. This phenomenon occurs as steel reinforcement reacts chemically with environmental elements such as water, oxygen, and chloride ions. When these elements penetrate concrete and reach the steel surface, they initiate and propagate corrosion. The rate of this deterioration, referred to as the corrosion rate, is a crucial parameter for assessing the durability and longevity of reinforced concrete structures. Typically expressed in micrometers per year ( $\mu\text{m}/\text{year}$ ), the corrosion rate indicates the speed at which steel reinforcement deteriorates due to environmental and chemical influences [1][2]. Numerous factors influence the corrosion rate of reinforcement steel. Among these, the compressive strength of concrete is a primary determinant as it affects the material's ability to resist cracking, thereby preventing the ingress of corrosive agents [3][4][5][6][7][8]. Similarly, tensile strength plays a vital role; higher tensile strength reduces the likelihood of crack formation, which limits pathways for aggressive substances to reach the steel [4][9]. Other significant factors include concrete permeability and sorptivity, which measure the material's capacity to resist or absorb moisture and harmful ions [10][11][12]. Alkalinity is another critical parameter; higher

pH levels in concrete can form a passive layer on the steel surface, offering protection against corrosion [13][14]. The composition of binder materials, particularly the inclusion of supplementary cementitious materials (SCMs) like silica fume, slag, and fly ash, also influences concrete durability by altering its microstructure and reducing permeability [15]. Lastly, the concentration of chloride ions plays a pivotal role, as high levels can break down the passive film on the steel surface, accelerating the corrosion process [15][16][17][18]. In this study, a comprehensive analysis of the factors affecting the corrosion rate of reinforcing steel was conducted. The relationships between variables such as penetration depth, alkalinity, compressive strength, tensile strength, and sorptivity were evaluated using the Statistical Package for the Social Sciences (SPSS), version 28.0. SPSS is a widely used statistical software that provides robust tools for data analysis and interpretation, making it highly suitable for engineering and scientific research. By employing SPSS, this study utilized Pearson correlation analysis to quantify the strength and direction of relationships between the selected factors and the corrosion rate. The statistical approach allowed for a systematic ranking of the variables based on their influence on corrosion, providing insights into the most critical factors for improving the durability of reinforced concrete structures. This investigation aims to offer valuable guidance for optimizing concrete mix designs by emphasizing the roles of mechanical properties,

permeability, and chemical composition in mitigating corrosion. Through the use of advanced statistical tools and in-depth analysis, this research contributes to the development of more durable and long-lasting reinforced concrete structures, particularly in aggressive environments.

## 2. RESEARCH SIGNIFICANCE

Corrosion of reinforcement steel within concrete structures is a well-documented issue in the literature, with numerous studies highlighting its detrimental impact on durability and lifespan. While previous research has explored various factors influencing corrosion rates, such as concrete compressive strength, permeability, and chloride concentration, there remains a need for a comprehensive analysis that ranks these factors based on their significance and impact. This study addresses this gap by employing Pearson correlation analysis to systematically rank the factors correlated with the corrosion rate of reinforcement steel. Unlike earlier works that focus on isolated factors, our research provides an integrated approach to understanding the corrosion process, offering a clearer picture of which factors are most critical to address when enhancing the durability of concrete structures. By utilizing a robust statistical method, the study introduces new insights and empirical evidence that can guide the development of more effective concrete mix designs and corrosion mitigation strategies. Thus, this research not only reinforces existing knowledge but also prioritizes the factors influencing corrosion, offering practical recommendations for improving the longevity and safety of concrete structures.

## 3. MATERIALS USED IN THE STUDY

A single kind of Ordinary Portland Cement (OPC) Grade 52.5 N, conforming to the Egyptian Standard Specification ES 4756-1/2021 [19], was utilized in this investigation. The materials used in the concrete mixtures were dolomite with a nominal maximum size of 10 millimeters, and the natural silica fume sand had known physical qualities and medium grading, conforming to the Egyptian Standard Specification ES 1109/2008 [20]. The study also made use of Addicrete BVF 1, a high-performance additive that lowers water

content while enhancing workability and strength in concrete, to further improve the material's qualities. The ASTM C 494 Type F [21], ES 1899/2008 [22]. 3.5% of the cement weight was administered as a dose. Addicrete BVF 1 can be pre-mixed with water or added during the mixing process. Its density at 25°C is  $1.18 \pm 0.01$  kg/L.

## 4. MIX PROPORTIONS

Fourteen series of Ordinary Portland Cement (OPC) mixtures were developed, varying in binder content (350, 450, 475, and 500 kg/m<sup>3</sup>) and water-to-cement ratios (0.25, 0.3, 0.28, and 0.5). These mixtures included three sets with fly ash replacing 10%, 20%, and 30% of the cementitious content, three sets with silica fume at the same replacement ratios, and three sets with slag also at comparable replacement ratios. Additionally, one high-strength mixture without silica fume and two high-strength mixtures with silica fume were created. Two OPC mixtures without any additives were also prepared: one served as a control, and the other had low compressive strength. Table 3 provides a detailed list of the components and mix proportions used in the investigation.

This study explored the use of varying proportions of supplementary cementitious materials (SCMs) in concrete, focusing on both high levels of silica fume (up to 30%) and lower proportions of slag to optimize the pozzolanic reaction, enhance durability, and balance strength development. By using higher silica fume content, the study aimed to achieve a denser microstructure and significantly reduce water permeability, addressing a gap in conventional research that typically examines lower silica fume levels (10-15%). In contrast, lower slag content was selected to ensure a complete reaction with calcium hydroxide during cement hydration, preventing unreacted particles and maintaining early strength. The research also compared the performance of these SCMs with fly ash, offering valuable insights into their impact on concrete performance and contributing to the development of high-performance, cost-effective concrete mixes.

**Table 1.** Chemical composition of the used Portland cement.

Compound	SiO <sub>2</sub>	CaO	Al <sub>2</sub> O <sub>3</sub>	Fe <sub>2</sub> O <sub>3</sub>	MgO	SO <sub>3</sub>	C <sub>3</sub> S	Na <sub>2</sub> O
Chemical composition%	20.55	60.95	5.35	3.62	1.03	2.81	35.10	0.523

**Table 2.** The chemical composition of the cementitious materials used.

Component	Silica Fume	Slag	Fly Ash
SiO <sub>2</sub>	97.79%	22%	50%
CaO	-	63%	5%
Al <sub>2</sub> O <sub>3</sub>	-	6%	25%
Fe <sub>2</sub> O <sub>3</sub>	-	4%	10%
MgO	-	3%	2%
CaSO <sub>4</sub>	-	2%	-
Other Oxides	2.21%	-	8%

**Table 3.** The components and mix proportions used in the investigation.

Mix Codes	Cement Content (Kg/m <sup>3</sup> )	Water (Liter/m <sup>3</sup> )	Coarse Aggregate (kg/m <sup>3</sup> )	Sand (Kg/m <sup>3</sup> )	Silica fume % Replacement	Fly Ash % Replacement	Slag % Replacement	W/C	S.P %
HPC-S1	427.5	148.39	1190	595	10%	0	0	0.284	3.50%
HPC-S2	360	135.54	1190.7	595.353	20%	0	0	0.25	3.50%
HPC-NS	500	125	1254	627	0	0	0	0.25	3.50%
CTRL	450	135	1291	646	0	0	0	0.3	3.50%
C350	350	175	1277	638.5	0	0	0	0.5	0%
S10	405	135	1291	646	0	0	10%	0.3	3.50%
S20	360	135	1291	646	0	0	20%	0.3	3.50%
S30	315	135	1291	646	0	0	30%	0.3	3.50%
F10	405	135	1291	646	0	10%	0	0.3	3.50%
F20	360	135	1291	646	0	20%	0	0.3	3.50%
F30	315	135	1291	646	0	30%	0	0.3	3.50%
SI10	405	135	1291	646	10%	0	0	0.3	3.50%
SI20	360	135	1291	646	20%	0	0	0.3	3.50%
SI30	315	135	1291	646	30%	0	0	0.3	3.50%

## 5. TESTS CONDUCTED IN THE STUDY

### 5.1 FRESH CONCRETE TESTS

In accordance with ASTM C143 [23], the slump test was performed on fresh concrete for all mixtures, and the results were recorded to evaluate the fresh concrete's properties and workability. This helped to clarify the effects of various admixtures and material proportions on the overall performance of the concrete.

### 5.2 CORROSION RATE MEASUREMENTS

As illustrated at figure (1), the corrosion rate of steel bars embedded in concrete was tested using cylindrical specimens with specific dimensions: 10 cm in diameter and 16 cm in height. In the center of each specimen, a steel rebar with a diameter of 16 mm and a height of 16 cm was placed, ensuring it was 42 mm from the base of the specimen to maintain consistent concrete cover around the reinforcement. The rebar extended 42 mm outside the specimen. The steel reinforcement was manufactured according to the specified chemical composition standards in the Egyptian Standards (ES 262/2009 Gr) [24] to ensure quality. All electrochemical measurements were carried out using VOLTA LAB version 1.11, produced by Radiometer Analytical, France. The tools and procedures included a saturated Ag/AgCl reference electrode, a Pt sheet counter electrode, and an HSS rebar as the working electrode. Potentiodynamic polarization measurements were performed in the potential range between -100 to +100 mV vs. OCPE (Open Circuit Potential Equilibrium) at a temperature of  $25 \pm 2$  °C with a scan rate of 1.0 mV/s. Electrochemical impedance spectra were recorded at the respective OCPE using AC signals with an amplitude of 5 mV peak-to-peak in the frequency range of

10 kHz to 10 MHz. NOVA 1.11 software (an advanced electrochemical analysis and data-fitting program) was used to record and fit the electrochemical measurements. Potentiodynamic polarization measurements were performed on high-strength rebar embedded in various concrete mixes, totaling 14 different mixes, after immersion in 3.5% NaCl solution for 360 days. Figure (2) shows the Sample Shape and figure (3) shows the Immersion Method, while figure (4) shows the Volta lab instrument.

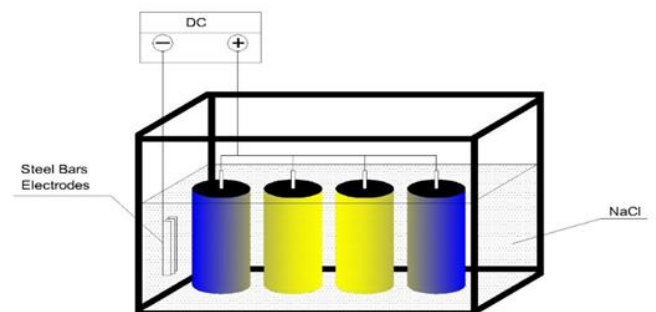
**FIGURE 1.** Schematic of the Method for Measuring Corrosion**FIGURE 2.** Sample Shape



FIGURE 3. Immersion Method



FIGURE 4. Volta Lab instrument

### 5.3 HARDENED CONCRETE TESTS

#### 5.3.1 PERMEABILITY TEST

After 28 days of curing, permeability testing was conducted on 15 cm cubic concrete samples. To measure the depth of water penetration into the concrete samples, water pressure was applied from underneath using the equipment specified in standard (ASTM C1202-18, 2012) [25]. Figure 5 shows the water pressure applied to the samples from below. After being dried in an oven at 105°C for 24 hours, the cubic concrete samples were exposed to water pressure from below for an additional 72 hours.



FIGURE 5. The water pressure applied to the samples

#### 5.3.2 SORPTIVITY TEST

According to ASTM C1585 [26], and as illustrated at figure (6), the test involved 100×50 mm concrete cylinders, with three samples from each mixture tested. Tests were conducted after 28 days of concrete curing. The samples were initially dried at 105°C until they reached a constant weight. The dried samples were weighed, then placed in water, submerged to a depth of 3 mm, and reweighed at set intervals to measure weight increase due to capillary water absorption. Samples were weighed every two hours. Sorptivity ( $S$ ) in (mm/min<sup>1/2</sup>) was calculated using the formula:

$$j = s \times \sqrt{t} + \alpha \quad (1)$$

Here,  $S$  is the sorptivity coefficient,  $t$  is time, and  $\alpha$  is a surface effect correction term (often not calculated). Total water intake ( $j$ ) was calculated with:

$$j = \Delta m / F \quad (2)$$

Where  $F$  is the sample surface area in contact with water, and  $\Delta m$  is the mass of absorbed water.



FIGURE 6. Sorptivity Test

#### 5.3.3 Alkalinity Test

To measure the alkalinity of concrete, a solution is made by mixing water with finely ground concrete powder, which is prepared by grinding a sample of concrete to increase its surface area for better dissolution. The powder is mixed with water to form a homogeneous solution, which is then filtered. The solution is poured onto filter paper in a filtration setup, which traps solid particles while the liquid containing dissolved alkaline compounds passes through. This liquid is collected and transferred to an alkalinity measurement device designed to accurately measure the alkalinity of solutions. The device quantifies the alkalinity level of the liquid sample, providing precise readings for accurate determination of the concrete's alkalinity. These measurements are recorded for further analysis and comparison, the procedure for this test was conducted according to ASTM E-15, 2015. [27]. Figure (7) shows the filtration process of the concrete solution.



FIGURE 7. The filtration process for the concrete solution

**5.3.4 COMPRESSIVE STRENGTH TEST**

The compressive strength test involves evaluating concrete samples. Each sample has dimensions of 15 × 15 × 15 cm. These tests are usually performed on the 28th day after casting and standard curing. For analysis, the average value from three cubes of each mix used in the study is taken [28].

**5.3.5 TENSILE STRENGTH TEST**

An indirect tensile strength test was performed using the splitting method on cylindrical concrete specimens with dimensions of 15 × 30 cm. This test was conducted on the 28th day after casting and curing. For analysis, the average value from three samples of each mix used in the study was recorded [29].

**6. RESULTS AND DISCUSSION**

**6.1 SLUMP TEST RESULT**

As illustrated at figure (8), the slump test results for concrete illustrate how different materials and their proportions affect workability. High-performance concrete containing silica fume (HPC-S1 and HPC-S2) exhibits lower slumps (6 cm and 7 cm) because the silica fume has a high surface area and absorbs the water and increases viscosity. In contrast, concrete without silica fume (HPC-NS) and the control mix (CTRL) show higher slumps (8 cm), indicating better workability. The mix with 350 kg/m<sup>3</sup> cement content (C350) achieves a slump of 9 cm, reflecting improved workability. Concrete with slag (S10, S20, and S30) shows a gradual increase in slump (9 cm, 10 cm, 11 cm) as the slag content increases. Similarly, concrete with fly ash (F10, F20, and F30) maintains a slump of 9 cm for F10 and F20 but increases to 11 cm for F30 because of having hydrophobic properties. Concrete with silica fume replacement (SI10, SI20, and SI30) demonstrates lower slumps (7 cm, 7 cm, 6 cm) due to increased viscosity and having a high surface area. Overall, adding silica fume decreases slump, while higher proportions of slag and fly ash improve workability, and increasing cement content also enhances it.

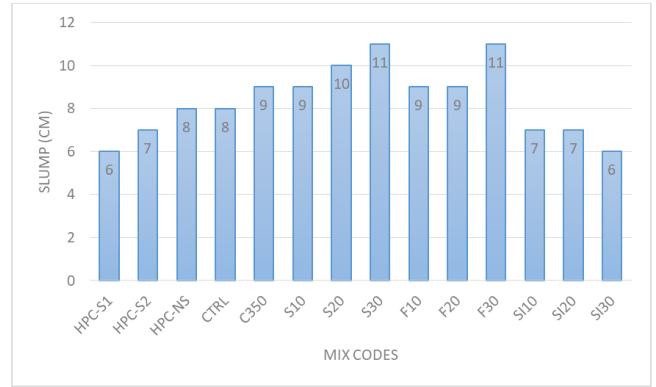


FIGURE 8. Results of the slump test

**6.2 CORROSION RATE MEASUREMENTS**

After measuring the corrosion rate using the Volta Lab device, three different values were obtained: the potential at which corrosion occurred (E) in millivolts (mV), the surface resistance of the steel to corrosion in kilo-ohm per square centimeter (kOhm·cm<sup>2</sup>), and the corrosion rate in micrometers per year (µm/year). Table 4 provides the values of corrosion rate, corrosion resistance.

Table 4. The values of corrosion rate, corrosion resistance, and potential

Mix codes	R (kOhm·cm <sup>2</sup> )	CR (µm/year)
HPC-S1	4.06	50.2
HPC-S2	7.92	36.96
HPC-NS	2.09	147.7
CTRL	2.15	145
C350	0.917	215.6
S10	2.2	142.4
S20	2.67	106.9
S30	3.97	77.99
F10	4.01	74.93
F20	4.71	74.93
F30	6.46	64.72
SI10	4.17	47.25
SI20	10.36	35.2
SI30	13.42	22.09

The results presented in the table indicate varying corrosion rates for the samples after immersion in sodium chloride solution. Mixes containing silica fume (SI10, SI20, and SI30) exhibited the lowest corrosion rates, with the SI30 mix showing a corrosion rate of 22.09 µm/year, while the SI10 and SI20 mixes had corrosion rates of 47.25 and 35.2 µm/year, respectively. On the other hand, the mixes containing slag (S10, S20, and S30) also showed good corrosion resistance, with corrosion rates ranging from 77.99 to 142.4 µm/year. The S30 mix demonstrated the best performance with a corrosion rate of 77.99 µm/year. The fly ash mixes (F10, F20, and F30) also showed good results, with corrosion rates ranging from 64.72 to 74.93 µm/year. The F30 mix exhibited the best performance within the fly ash group with a corrosion rate of 64.72 µm/year. The HPC-S2 mix, which contains a higher percentage of silica fume, showed the best performance within the high performance group, with a corrosion rate of 36.96 µm/year. In contrast, the HPC-S1 mix showed a slightly higher corrosion rate of

50.2  $\mu\text{m}/\text{year}$ . The HPC-NS mix, which does not contain silica fume, exhibited the highest corrosion rate within the high performance group at 147.7  $\mu\text{m}/\text{year}$ , followed by the CTRL (control) mix with a corrosion rate of 145  $\mu\text{m}/\text{year}$ .

The C350 mix showed the highest corrosion rate among all mixes, at 215.6  $\mu\text{m}/\text{year}$ , reflecting the impact of the additional materials in improving the concrete's corrosion resistance. The interpretation of these results is based on the microstructural improvements and pozzolanic activity provided by the supplementary cementitious materials. Silica fume, slag, and fly ash all help improve the concrete's structure and reduce permeability, thus enhancing the corrosion resistance of the concrete. [30]. It is observed that as corrosion resistance increases, the corrosion rate decreases, as illustrated in the following figure (9).

Figure (10) shows the potential induced by corrosion for each sample.

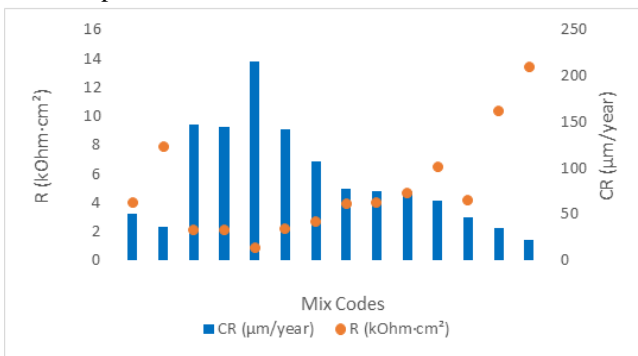


FIGURE 9. Corrosion Rate vs. Corrosion Resistance

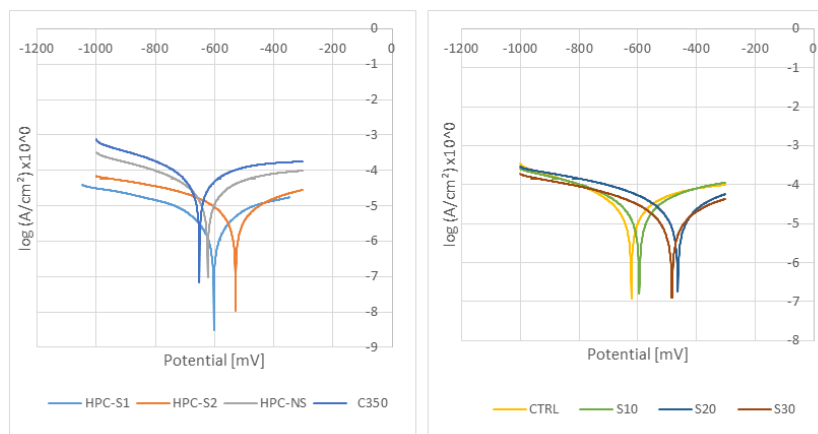
Figure 10 illustrates the electrochemical response of various concrete mixes, highlighting the relationship between the potential induced by corrosion and the composition of each mix. The figure shows how each mix's composition affects its resistance to chloride-induced corrosion. Mixes incorporating supplementary cementitious materials, such as silica fume, fly ash, and slag, demonstrate lower corrosion potentials, indicating enhanced resistance. For instance, the silica fume-based mixes (SI10, SI20, and SI30) show significantly lower potentials, reflecting their ability to create a denser microstructure and reduce chloride ingress. Similarly, fly ash mixes, particularly F30, exhibit improved performance with lower potential values due to the spherical shape of fly ash particles, which improve

workability and reduce permeability. On the other hand, mixes with traditional cement content, such as CTRL and HPC-NS, exhibit higher corrosion potentials, indicating a greater susceptibility to chloride-induced corrosion. This can be attributed to their less dense microstructure, which allows for increased chloride ingress. Consequently, these mixes show higher corrosion rates and reduced durability, as they do not benefit from the protective effects of supplementary cementitious materials, like silica fume, fly ash, or slag, which enhance the concrete's resistance to corrosion.

This comparison underscores the role of mix composition in mitigating corrosion and prolonging the service life of reinforced concrete structures.

### 6.3 RESULTS OF HARDENED CONCRETE PROPERTIES TESTS

Table 5 presents the results of various concrete mixes in terms of compressive strength, tensile strength, penetration depth, sorptivity, and alkalinity after 28 days of curing. Among the silica-based mixes, SI30 shows the highest compressive strength (840  $\text{kg}/\text{cm}^2$ ) and tensile strength (67.2  $\text{kg}/\text{cm}^2$ ), along with the lowest penetration depth (2 mm), indicating the best performance in terms of durability. Regarding the slag-based mixes, S30 offers the best balance between durability and strength, with a penetration depth of 11.25 mm and a sorptivity value of  $11.2 \times 10^{-5}$  ( $\text{mm}/\sqrt{\text{s}}$ ). While S10 and S20 show relatively higher penetration depths (16.25 mm and 15 mm, respectively), S30 stands out with improved resistance to chloride ingress and water absorption, making it the most efficient slag mix in terms of overall performance. The C350 mix, however, shows the weakest performance with a low compressive strength of 327  $\text{kg}/\text{cm}^2$  and the highest penetration depth of 34.38 mm, indicating poor resistance to chloride ingress and water absorption. The control mix (CTRL) and the HPC-NS mix show lower overall performance, with higher penetration depths and sorptivity values, indicating weaker resistance to chloride ingress. The alkalinity values remain relatively consistent across the mixes, with slight variations, indicating that all mixes maintain a similar pH level. This data highlights the importance of supplementary cementitious materials, particularly silica fume, in enhancing concrete durability, while slag and fly ash also improve specific properties such as workability and corrosion resistance.



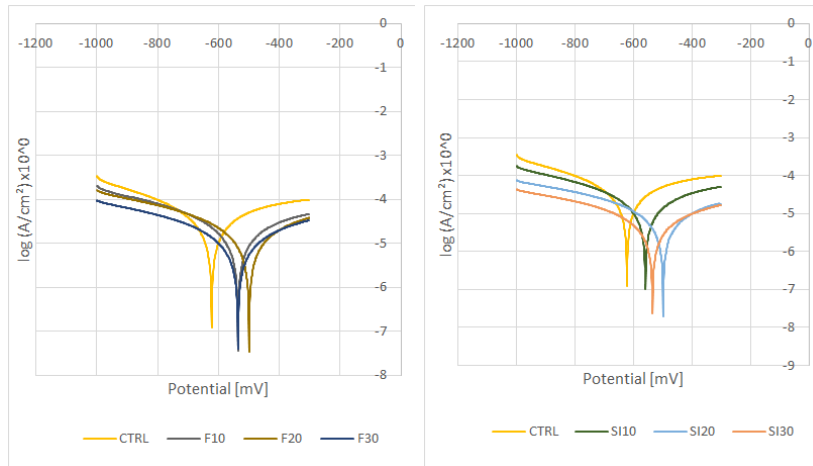


FIGURE 10. Electrochemical Response of Various Concrete Mixes Showing Corrosion-Induced Potential

Table 5. Results of Hardened Concrete Properties Testing

Mix codes	Compressive Strength at 28 d (kg/cm <sup>2</sup> )	Tensile Strength at 28 d (kg/cm <sup>2</sup> )	Penetration Depth (mm)	Sorptivity × 10 <sup>-5</sup> (mm <sup>2</sup> /√s)	Alkalinity
HPC-S1	812	63.88	3	5.999	13.68
HPC-S2	678	46.7	9.38	7.47	13.6
HPC-NS	600	28.34	10	8.38	13.94
CTRL	386.2	22.4	18.75	7.23	12.9
C350	327	20.6	34.38	19.55	13
S10	422	23.44	16.25	13.8	13.4
S20	474	22.75	15	13.4	13.4
S30	497.7	25.4	11.25	11.2	13.2
F10	392.7	18.82	16.25	14	13.2
F20	442	22	16.88	5.89	13.11
F30	450	19.11	14.38	4.27	13.3
SI10	604	33.582	10	10.500	13.6
SI20	689	41.64	9.38	6.150	13.8
SI30	840	67.2	2	4.750	13.8

7. R-SQUARED AND PEARSON CORRELATION

Pearson Correlation (r) measures the strength and direction of the linear relationship between two variables, providing a value between -1 and +1. A value of +1 indicates a perfect positive correlation (both variables increase together), -1 indicates a perfect negative correlation (one variable increases while the other decreases), and 0 indicates no linear correlation. Pearson correlation helps determine how closely the two variables move together.

On the other hand, R<sup>2</sup> (R-squared) represents the percentage of variance in the dependent variable that can be explained by the independent variables in the model. When R<sup>2</sup> is used in a simple linear regression model (with one

independent variable), it is the square of the Pearson correlation coefficient. R<sup>2</sup> values range from 0 to 1, where a value of 1 indicates that the model explains 100% of the variance, and a value of 0 indicates that the model explains none of the variance. Therefore, R<sup>2</sup> is a key metric for evaluating how well the model fits the data.

If the model contains multiple independent variables, R<sup>2</sup> reflects the combined ability of all these variables to explain the variance in the dependent variable. Unlike Pearson correlation, which measures the relationship between two variables only, R<sup>2</sup> in multiple regression models reflects the contribution of many independent variables to explaining the variance in the dependent variable. This is particularly useful

in complex models with multiple independent variables, as  $R^2$  provides a summary of the model's explanatory power.

It is important to note that in some cases, a low  $R^2$  value may still be acceptable, especially when the relationship between the variables is complex and influenced by multiple factors. Therefore,  $R^2$  should not be the sole criterion for judging the quality of the model; the scientific context must also be considered. [31]

### 7.1 CORROSION RATE VS. COMPRESSIVE STRENGTH

Figure 11 shows a clear relationship between the compressive strength and corrosion resistance of the concrete mixes. The mixes with higher compressive strengths, such as SI30 (840 kg/cm<sup>2</sup>), exhibit significantly lower corrosion rates (22.09  $\mu\text{m}/\text{year}$ ), indicating better resistance to chloride-induced corrosion. In contrast, mixes like HPC-NS (600 kg/cm<sup>2</sup>) and C350 (327 kg/cm<sup>2</sup>) show higher corrosion rates (147.7 and 215.6  $\mu\text{m}/\text{year}$ , respectively), suggesting a lower resistance to corrosion. The addition of supplementary materials like silica fume (SI10, SI20, and SI30) and slag (S10, S20, and S30) improves the corrosion resistance, with SI30 showing the best performance within all mixes. On the other hand, mixes containing fly ash (F10, F20, F30) also exhibit improved corrosion resistance, with F30 having a corrosion rate of 64.72  $\mu\text{m}/\text{year}$ . These findings highlight the importance of both compressive strength and the use of supplementary materials in enhancing the durability of concrete exposed to chlorides. The linear regression with (R square) value of 0.4846 suggests a moderate negative correlation between the variables. The scatter plot would likely show a downward trend, where as one variable increases, the other decreases, but the data points are somewhat dispersed around the line, reflecting the R square value. This indicates that while there is a general relationship between the two variables, a significant portion of the variation is not explained by the model. The moderate R square value implies that other factors may influence the observed data [32].

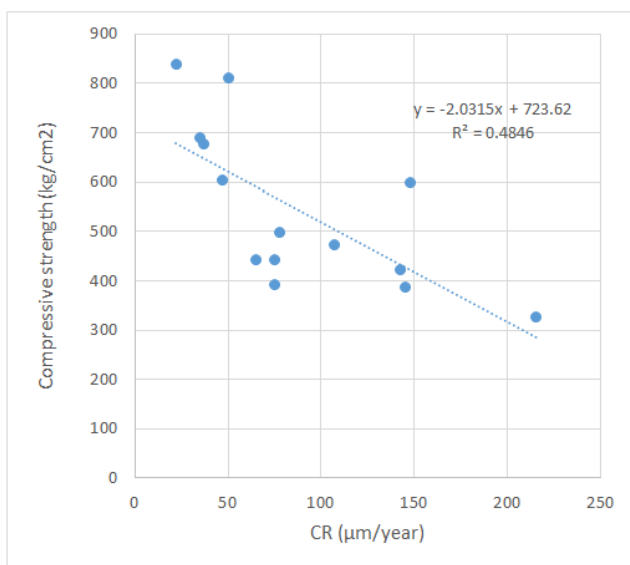


FIGURE 11. Corrosion Rate vs. Compressive strength

### 7.2 CORROSION RATE VS. TENSILE STRENGTH

Figure 12 shows the scatter plot of the relationship between tensile strength and corrosion rate (CR) indicates a moderate negative correlation. As tensile strength increases, the corrosion rate tends to decrease, suggesting that higher tensile strength in the concrete mixes leads to improved resistance to corrosion. For example, mixes like SI30, with higher tensile strength (67.2 kg/cm<sup>2</sup>), exhibit significantly lower corrosion rates (22.09  $\mu\text{m}/\text{year}$ ), while mixes with lower tensile strength, such as C350 (20.6 kg/cm<sup>2</sup>), show higher corrosion rates (215.6  $\mu\text{m}/\text{year}$ ). However, the data points are somewhat spread out around the trend line, reflecting the  $R^2$  value of 0.3589, which means that while tensile strength explains about 36% of the variance in corrosion rate, other factors likely influence the observed data. This moderate correlation highlights the importance of tensile strength, but also indicates that additional variables may play a significant role in the corrosion behavior of concrete [33].

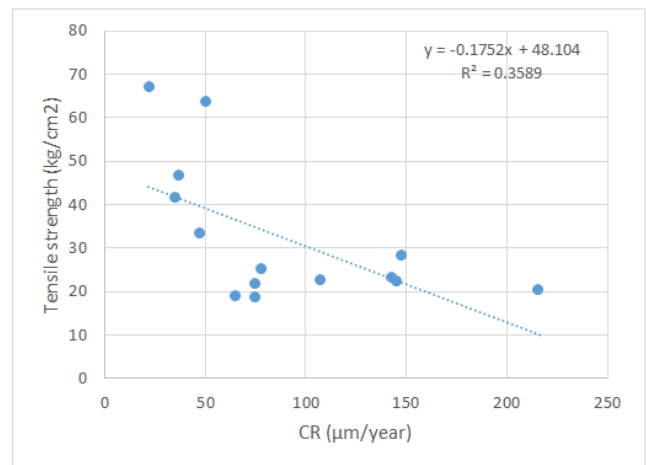


FIGURE 12. Corrosion Rate vs. Tensile strength

### 7.3 CORROSION RATE VS. PENETRATION DEPTH

Figure 13 shows the scatter plot of the relationship between penetration depth and corrosion rate (CR) indicates a moderate positive correlation. As the penetration depth increases, the corrosion rate also tends to increase, suggesting that greater penetration of chloride ions into the concrete leads to higher rates of corrosion. For example, mixes like C350, with a deeper penetration depth (34.38 mm), show a significantly higher corrosion rate (215.6  $\mu\text{m}/\text{year}$ ), while mixes with shallower penetration depths, such as SI30 (2 mm), exhibit much lower corrosion rates (22.09  $\mu\text{m}/\text{year}$ ). The data points are relatively well aligned with the trend line, reflecting the  $R^2$  value of 0.6533, which indicates that approximately 65.33% of the variance in corrosion rate can be explained by penetration depth. This strong correlation suggests that penetration depth is a key factor influencing corrosion behavior, although other variables may still contribute to the overall corrosion process [34].

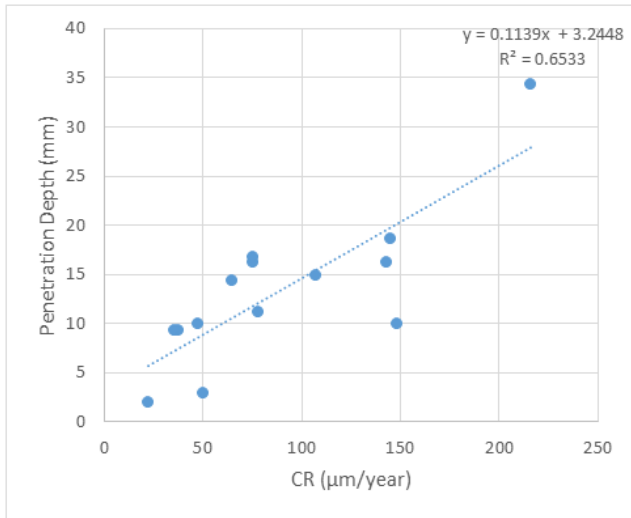


FIGURE 13. Corrosion Rate vs. Penetration Depth

7.4 CORROSION RATE VS SORPTIVITY

The scatter plot in Figure 14 shows the relationship between sorptivity and corrosion rate (CR), illustrating a positive but relatively moderate correlation. As sorptivity increases, the corrosion rate also tends to increase, indicating that higher water absorption rates in concrete lead to greater corrosion of the reinforcement. For example, mixes like C350, with higher sorptivity values ( $19.55 \times 10^{-5}$  mm/√s), exhibit higher corrosion rates (215.6 μm/year), while mixes with lower sorptivity, such as F30 ( $4.27 \times 10^{-5}$  mm/√s), show significantly lower corrosion rates (64.72 μm/year). The data points generally follow the trend line, as reflected by the R<sup>2</sup> value of 0.4588, which suggests that about 46% of the variation in corrosion rate can be explained by sorptivity. This moderate correlation suggests that while sorptivity is a contributing factor to the corrosion process, other factors may also play a role in influencing the overall corrosion behavior of the concrete [35].

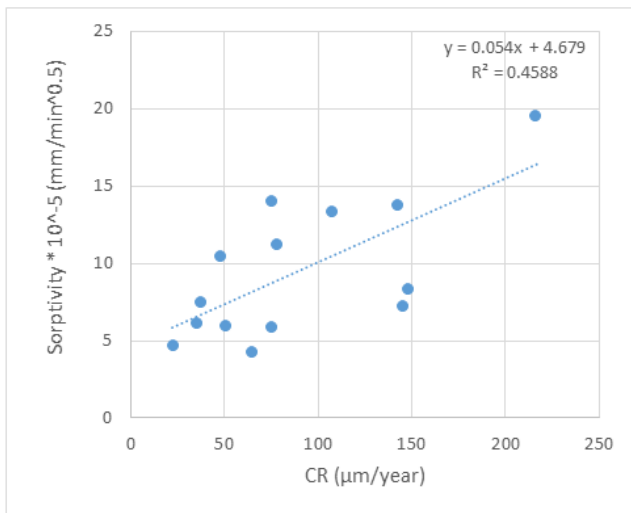


FIGURE 14. Corrosion Rate vs. sorptivity

7.5 CORROSION RATE VS ALKALINITY

Based on the provided scatter plot (Figure 15), which shows the relationship between alkalinity and corrosion rate

(CR), the alkalinity values were analyzed as a nominal variable and categorized into three ranges: 12.5–13 (represented as 1), 13.1–13.5 (represented as 2), and 13.6–14 (represented as 3). The results indicate a negative correlation between alkalinity and corrosion rate. As the alkalinity category increases slightly, the corrosion rate tends to decrease, suggesting that higher alkalinity may offer some protection against corrosion. The R<sup>2</sup> value is 0.5127, indicating that about 51% of the variance in corrosion rate can be explained by the alkalinity categories, suggesting a moderate relationship.

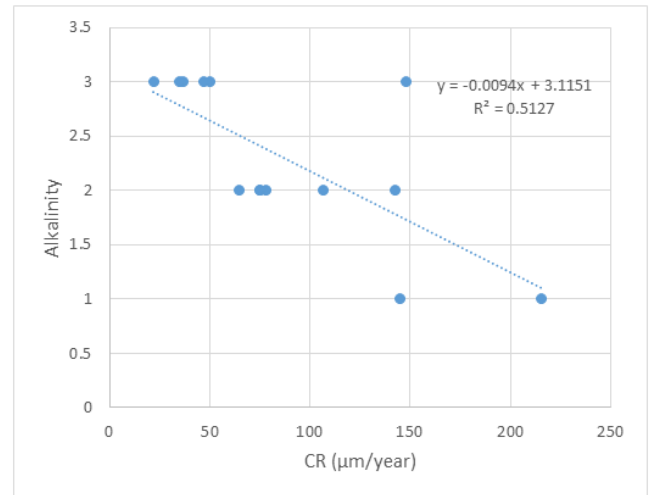


Figure 15. Corrosion Rate vs. Alkalinity

7.6 PEARSON CORRELATION MODEL

As illustrated in Table 6, the Pearson correlation analysis examined the relationship between the corrosion rate and various independent variables, including penetration depth, alkalinity, compressive strength, sorptivity, and tensile strength using the SPSS software program. The results showed that penetration depth had the greatest impact on corrosion, with ( $r = 0.808$ ,  $R^2 = 0.6533$ ) and a highly significant p-value ( $p < 0.001$ ), explaining 65.33% of the variation in the corrosion rate. This indicates a strong positive correlation between penetration depth and corrosion rate, highlighting its critical role in allowing chloride ingress. Alkalinity followed, with ( $r = -0.716$ ,  $R^2 = 0.5127$ ) and a significant p-value ( $p = 0.004$ ), accounting for 51.27% of the variation in corrosion rate. This suggests a strong negative correlation between alkalinity and corrosion, meaning that a high-pH environment contributes to reducing corrosion by protecting against chloride interaction. Compressive strength had ( $r = -0.696$ ,  $R^2 = 0.4846$ ) with a significant p-value ( $p = 0.006$ ), explaining 48.46% of the variation. This highlights the importance of concrete strength in reducing pathways for corrosive agents. Sorptivity showed ( $r = 0.677$ ,  $R^2 = 0.4588$ ) with a significant p-value ( $p = 0.008$ ), contributing to 45.88% of the variation. This indicates that increased water absorption leads to higher corrosion risks, as water facilitates chloride ingress. Tensile strength had the least impact, with ( $r = -0.599$ ,  $R^2 = 0.3589$ ) and a significant p-value ( $p = 0.024$ ), explaining 35.89% of the variation. This reflects its smaller but still meaningful role in minimizing cracks that contribute to corrosion. The overall model had an R<sup>2</sup> of

0.719, indicating that 71.9% of the variation in the corrosion rate can be explained by these variables. This analysis underscores the importance of targeting penetration depth

and alkalinity in concrete mix designs to enhance corrosion resistance and durability.

**Table 6.** Correlation Coefficients and Explained Variance ( $R^2$ ) for Variables Influencing Corrosion Rate

Variables	Penetration depth	Alkalinity	Compressive Strength	Sorptivity	Tensile Strength
Corrosion Rate	Pearson correlation				
	0.808	-0.716	-0.696	0.677	-0.599
	Sig. (2-tailed)				
	0.000	0.004	0.006	0.008	0.024
	$R^2$				
	0.6533	0.5127	0.4846	0.4588	0.3589
	Model $R^2 = 0.719$				

## 8. Conclusion

This study provides valuable insights into the factors influencing the corrosion rate of steel reinforcement in concrete. The analysis of various variables such as penetration depth, alkalinity, compressive strength, tensile strength, and sorptivity, using Pearson correlation coefficients, helps to highlight their respective roles in mitigating or accelerating corrosion. The key findings are summarized below:

- Penetration depth is the most influential factor in accelerating corrosion, with a strong positive correlation with the corrosion rate ( $r = 0.808$ ,  $R^2 = 0.6533$ ,  $p = 0.000$ ), indicating that increased penetration depth significantly raises corrosion due to chloride ingress.
- Alkalinity showed the strongest negative correlation ( $r = -0.716$ ,  $R^2 = 0.2368$ ,  $p = 0.004$ ), demonstrating its protective effect by maintaining a high pH environment that supports the passive layer on the steel surface.
- Compressive strength also demonstrated a significant negative correlation with the corrosion rate ( $r = -0.696$ ,  $R^2 = 0.4846$ ,  $p = 0.006$ ), suggesting that stronger concrete reduces pathways for corrosive agents and thus mitigates corrosion.
- Tensile strength exhibited a moderate negative correlation ( $r = -0.599$ ,  $R^2 = 0.3589$ ,  $p = 0.024$ ), highlighting its contribution to limiting crack formation and reducing corrosion.
- Sorptivity showed a moderate positive correlation ( $r = 0.677$ ,  $R^2 = 0.4588$ ,  $p = 0.008$ ), indicating that increased water absorption in concrete leads to higher corrosion, though the effect is less pronounced compared to penetration depth.
- Concrete mixes with supplementary cementitious materials (SCMs) like silica fume and fly ash significantly enhanced corrosion resistance. For example, the SI30 mix showed the lowest corrosion rate (22.09  $\mu\text{m}/\text{year}$ ) due to its dense microstructure and reduced permeability.
- The C350 mix, with higher water-to-cement ratios and lower SCM content, exhibited the highest corrosion rate (215.6  $\mu\text{m}/\text{year}$ ), emphasizing the negative impact of higher porosity on corrosion resistance.

- Optimizing concrete mix designs by prioritizing factors such as reduced penetration depth, increased alkalinity, and improved mechanical properties is essential to enhance corrosion resistance and extend the service life of reinforced concrete structures.
- This study provides valuable insights for developing effective strategies to mitigate corrosion in reinforced concrete by improvement the selecting of the materials and mix design, thereby increasing the durability and longevity of structures.
- Concrete mixes containing slag, particularly the S30 mix, demonstrated a balanced improvement in durability and mechanical properties. The S30 mix exhibited a significant reduction in penetration depth (11.25 mm) and sorptivity ( $11.2 \times 10^{-5} \text{ mm}/\sqrt{\text{s}}$ ) compared to other slag mixes, highlighting its superior resistance to chloride ingress and water absorption. These results emphasize the potential of slag as a supplementary cementitious material in enhancing the long-term durability and corrosion resistance of concrete, making it a viable option for structures exposed to aggressive environments.

## REFERENCES

- [1] Page, Chris L., and Mary M. Page, eds. *Durability of concrete and cement composites*. Elsevier, 2007.
- [2] Broomfield, John P. *Corrosion of steel in concrete: understanding, investigation and repair*. Crc Press, 2023.
- [3] Mehta, Povindar K., and Paulo Monteiro. "Concrete: microstructure, properties, and materials." (No Title) (2006).
- [4] Tuutti, Kyösti. "Corrosion of steel in concrete." (1982).
- [5] Ismail, Mohamed, and Masayasu Ohtsu. "Corrosion rate of ordinary and high-performance concrete subjected to chloride attack by AC impedance spectroscopy." *Construction and Building Materials* 20.7 (2006): 458-469.
- [6] Prabowo, H. "Durability based service life prediction of bacterial concrete." *Journal of Physics: Conference Series*. Vol. 1469. No. 1. IOP Publishing, 2020.
- [7] Rashid, Muhammad Harunur, et al. "Effect of strength and covering on concrete corrosion." *European Journal of Scientific Research* 40.4 (2010): 492-499.
- [8] Kotes, P., M. Strieska, and M. Brodnan. "Sensitive analysis of calculation of corrosion rate according to standard approach." *IOP Conference Series: Materials Science and Engineering*. Vol. 385. No. 1. IOP Publishing, 2018.

- [9] Chernin, Leonid. Effect of corrosion on the concrete-reinforcement interaction in reinforced concrete beams. Technion-Israel Institute of Technology, Faculty of Civil and Environmental Engineering, 2008.
- [10] Yu, Xianzheng, et al. "Research on the Permeability and Pore Structure Distribution Characteristics of High-Performance Mortar for Surface Treatment of Bridge Piers and Columns." *Buildings* 14.3 (2024): 811.
- [11] Williamson, S. J., and L. A. Clark. "The influence of the permeability of concrete cover on reinforcement corrosion." *Magazine of Concrete Research* 53.3 (2001): 183-195.
- [12] Singh, Yuvraj, and Harvinder Singh. "Influence of steel fibres on the sorptivity of corroded reinforced concrete." *International Journal of Design Engineering* 12.1 (2023): 30-48.
- [13] Perks, Robert Adam. Chloride thresholds for initiation of corrosion of steel reinforcement in concrete. Florida Atlantic University, 2000.
- [14] Nam, Jingak. Effects of cement alkalinity, exposure conditions and steel-concrete interface on the time-to-corrosion and chloride threshold for reinforcing steel in concrete. Florida Atlantic University, 2004.
- [15] Phuong, D. T. V., et al. "Effects of w/b ratio, fly ash, and chloride content on corrosion of reinforcing steel." *IOP Conference Series: Materials Science and Engineering*. Vol. 615. No. 1. IOP Publishing, 2019.
- [16] Güneyisi, Erhan, et al. "Corrosion behavior of reinforcing steel embedded in chloride contaminated concretes with and without metakaolin." *Composites Part B: Engineering* 45.1 (2013): 1288-1295.
- [17] AL-ATTAR, Tareq Salih. "EFFECT OF CHLORIDE IONS SOURCE ON CORROSION OF REINFORCED NORMAL AND HIGH PERFORMANCE CONCRETE."
- [18] Thangavel, K., and N. S. Rengaswamy. "Relationship between chloride/hydroxide ratio and corrosion rate of steel in concrete." *Cement and concrete Composites* 20.4 (1998): 283-292.
- [19] Egyptian Standards (ES) 4756-1/2021, "Ordinary Portland Cement - Composition, Specifications, and Conformity Criteria," Egyptian Organization for Standardization and Quality, Cairo, Egypt, 2021.
- [20] Egyptian Standards (ES) 1109/2008, "Aggregates for Concrete - Specifications," Egyptian Organization for Standardization and Quality, Cairo, Egypt, 2008.
- [21] ASTM C494/C494M-18, "Standard Specification for Chemical Admixtures for Concrete," ASTM International, West Conshohocken, PA, USA, 2018.
- [22] Egyptian Standards (ES) 1899/2008, "Additives for Concrete - Requirements and Testing Methods," Egyptian Organization for Standardization and Quality, Cairo, Egypt, 2008.
- [23] ASTM C143. "Standard Test Method for Slump of Hydraulic-Cement Concrete." *Annual Book of ASTM Standards*, Vol. 04.02, 1998, pp. 283-292.
- [24] Egyptian Standards (ES) 262/2009 Gr, "Reinforcing Steel Bars for Concrete - Specifications," Egyptian Organization for Standardization and Quality, Cairo, Egypt, 2009.
- [25] ASTM, C. "Standard test method for electrical indication of concrete's ability to resist chloride ion penetration." C1202-18 (2012).
- [26] ASTM C1585 - Standard Test Method for Measurement of Rate of Absorption of Water by Hydraulic-Cement Concretes.
- [27] ASTM Committee E-15 on Industrial and Specialty Chemicals. Standard test method for pH of aqueous solutions with the glass electrode. ASTM International, 2015.
- [28] ASTM C109/C109M-02, Standard Test Method for Compressive Strength of Hydraulic Cement Mortars (Using 2-in. Or 50 mm Cube Specimens)
- [29] ASTM C496/C496M-11, 2011 Standard Test Method for Splitting Tensile Strength of Cylindrical Concrete Specimen, August 2011.
- [30] Diamond, Sidney. "Effects of microsilica (silica fume) on pore-resolution chemistry of cement pastes." *Journal of the American Ceramic Society* 66.5 (1983): C-82.
- [31] Field, Andy. *Discovering statistics using IBM SPSS statistics*. Sage publications limited, 2024.
- [32] Bremner, Theodore, et al. "Protection of metals in concrete against corrosion." Technical Report for ACI Committee 222: Farmington Hills, MI, USA. 2001.
- [33] Dyer, Thomas. *Concrete durability*. Crc Press, 2014.
- [34] Ahmad, Zaki. *Principles of corrosion engineering and corrosion control*. Elsevier, 2006.
- [35] Kayali, O., and B. Zhu. "Corrosion performance of medium-strength and silica fume high-strength reinforced concrete in a chloride solution." *Cement and Concrete Composites* 27.1 (2005): 117-124.